Environmental Science & Technology

Article

pubs.acs.org/est

Synthesis of Size-Tunable CO_2-Philic Imprinted Polymeric Particles (MIPs) for Low-Pressure CO_2 Capture Using Oil-in-Oil Suspension Polymerization

Seyed Ali Nabavi,[†,‡] Goran T. Vladisavljević,*[,†] Yidi Zhu,[†] and Vasilije Manović*[,‡]

[†]Department of Chemical Engineering, Loughborough University, Loughborough, LE11 3TU, United Kingdom

[‡]Combustion and CCS Centre, Cranfield University, Cranfield, MK43 0AL, United Kingdom

Supporting Information

ABSTRACT: Highly selective molecularly imprinted poly-[acrylamide-*co*-(ethylene glycol dimethacrylate)] polymer particles (MIPs) for CO_2 capture were synthesized by suspension polymerization via oil-in-oil emulsion. Creation of CO_2-philic, amide-decorated cavities in the polymer matrix led to a high affinity to CO_2. At 0.15 bar CO_2 partial pressure, the CO_2/N_2 selectivity was 49 (corresponding to 91% purity of the gas stream after regeneration), and reached 97 at ultralow CO_2 partial pressures. The imprinted polymers showed considerably higher CO_2 uptakes compared to their nonimprinted counterparts, and the maximum equilibrium CO_2 capture capacity of 1.1 mmol g^{-1} was achieved at 273 K. The heat of adsorption was below 32 kJ mol^{-1} and the temperature of onset of intense thermal degradation was 351−376 °C. An increase in monomer-to-cross-linker molar ratio in the dispersed phase up to 1:2.5 led to a higher affinity toward CO_2 due to higher density of selective amide groups in the polymer network. MIPs are a promising option for industrial packed and fluidized bed CO_2 capture systems due to large particles with a diameter up to 1200 μm and irregular oblong shapes formed due to arrested coalescence during polymerization, occurring as a result of internal elasticity of the partially polymerized semisolid drops.

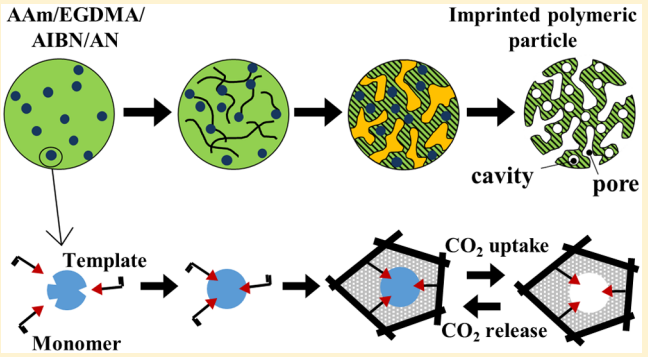

1. INTRODUCTION

In accordance with the Climate Change Act 2008, the UK Government has targeted to achieve at least 80% reduction in the emission of CO_2 and other greenhouse gases (GHGs), from the 1990 baseline, by 2050.[1] The power sector is one of the major GHG emitters and accounts for nearly 60% of global CO_2 emissions.[2] In addition, industrial sectors are responsible for almost 25% of total global CO_2 emissions.[3] Carbon capture and storage (CCS) has been identified as the key mitigation strategy for decarbonisation of power and industrial sectors, in order to minimize climate change.[4] It is reported that CCS alone can contribute to almost 19% of emission reduction by 2050,[1] and the exclusion of CCS could increase the global cost of achieving the emission reduction target by 70%.[5] CO_2 capture is the first and most expensive step in the CCS chain. The main technologies for CO_2 capture are precombustion, postcombustion, and oxy-combustion.[6] Among them, postcombustion capture is considered as the most feasible short-to-medium term strategy, since it can be retrofitted to existing power plants without any extensive modification.[7]

Monoethanolamine (MEA) scrubbing is a mature form of postcombustion capture and is considered as the benchmark technology for CO_2 capture.[8] Although MEA is inexpensive and has a relatively high CO_2 capture capacity, it is corrosive and undergoes degradation in the presence of flue gas impurities and at elevated temperatures, which raises environmental concerns.[9,10] The main drawback of MEA is associated with a high amount of energy required for its regeneration that imposes a significant energy penalty on power plants.[7]

Solid adsorbents, such as metal−organic frameworks (MOFs), zeolites, polymers, activated carbons, and amine-functionalized silicas, can be promising alternatives to the conventional amine-based solvents, because of their low energy requirements and minimal corrosivity.[11,12] The key criteria for selecting an ideal adsorbent for low-temperature postcombustion capture are (1) low heat of adsorption; (2) high working capacity; (3) high CO_2 selectivity; (4) high hydrochemical, thermal, and mechanical stability; (5) high recyclability; (6) production scalability; (7) optimum morphology; (8) low cost; and (9) low toxicity and corrosivity.[7,11,13−15] In the chemisorption process, the adsorbates and adsorbents make covalent bonds and the heat of adsorption is larger than 40 kJ mol^{-1}. Physisorptive adsorbents, such as polymers, do not form

Received: June 28, 2017
Revised: September 7, 2017
Accepted: September 8, 2017
Published: September 8, 2017

DOI: 10.1021/acs.est.7b03259
Environ. Sci. Technol. 2017, 51, 11476−11483

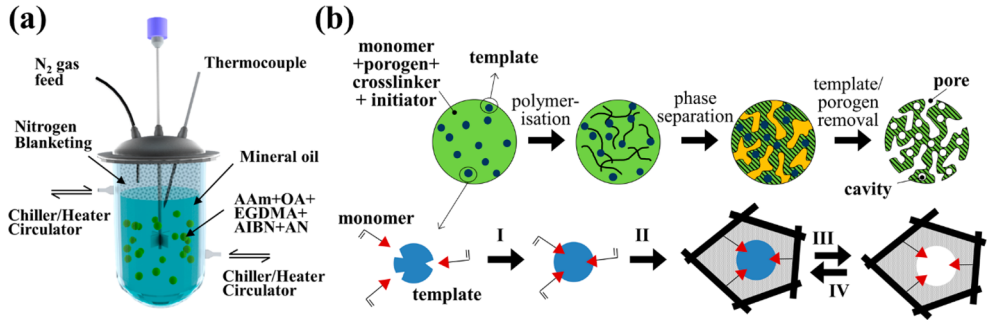

Figure 1. (a) Schematic of the jacketed reactor used for O/O suspension polymerization. (b) Steps in the synthesis of MIPs: I. OA-AAm self-assembly via hydrogen bonding and formation of prepolymerization complex in the organic phase; II. copolymerization with EGDMA; III. template removal, IV. adsorption of CO_2 molecules within the cavities.

chemical bonds with CO_2 resulting in the heat of adsorption below 40 kJ mol^{-1}.[16] Thus, they incur lower energy penalties and can be considered as a promising alternative to MEA, if they meet the aforementioned performance requirements.

One of the key disadvantages of physisorptive adsorbents is their low affinity toward CO_2 (low CO_2selectivity). For example, Mg-MOF-74,[17,18] Zeolite 13X,[19] and COP-4 (covalent organic polymer)[20] demonstrated a significant CO_2 adsorption capacity in simulated postcombustion conditions, but suffered from relatively low CO_2/N_2 selectivity. Moreover, the morphology and production scalability of the adsorbents are other important issues that have often been neglected.[21] The majority of adsorbents are produced as fine powders that are not practical for use in industrial CO_2 capture systems.[15,18,22] Thus, they must be pelletized, which may alter their performance and increase production costs.

Zhao et al.[23,24] developed molecularly imprinted polymer (MIP) particles by creating amide-decorated cavities with CO_2 recognition properties within the polymer network, using bulk polymerization. The MIP particles benefited from high CO_2/N_2 selectivity, high thermal stability, and low sensitivity to SO_2, NO, O_2, and moisture. However, in bulk polymerization, the monolithic polymers need to be ground and sieved to the desired size range, which is time-consuming and laborious, with only 30−40% of the particles recovered. In addition, the produced particles are susceptible to attrition due to their irregular shape with sharp corners and thus, they suffer from high degradation rates.[25]

Suspension polymerization is an alternative approach for synthesizing MIP particles. This process is commercially scalable and benefits from efficient removal of the heat released during polymerization. Since the particle size can be controlled by stirring rate, there is no need for sieving and the process generates less waste. Furthermore, the synthesized particles have a spherical morphology and are less prone to attrition.[25−27] In conventional oil-in-water (O/W) or water-in-oil (W/O) suspension polymerization routes, the presence of water can weaken the template-monomer interactions. Moreover, a stabilizer added to the continuous phase to prevent droplet coalescence can act as an impurity and impact the performance of the particles.[15,25] Oil-in-oil (O/O) suspension polymerization route can be applied to eliminate both water and stabilizers from the process.[28,29]

In this work, a series of novel oxalic acid imprinted poly(AAm-*co*-EGDMA) beads with tuned morphology were synthesized using the O/O suspension polymerization approach. The polymeric beads were inherently amide functionalized and showed a high selectivity to CO_2 over N_2. Comprehensive physicochemical characterization has been carried out to assess the performance of the synthesized materials in typical temperature swing adsorption scenarios. High CO_2 selectivity, production scalability, low heat of adsorption, and optimum particle morphology make MIP adsorbents promising candidates for postcombustion CO_2 capture.

2. EXPERIMENTAL SECTION

2.1. Materials. Oxalic acid (OA), acrylamide (AAm), light mineral oil, acetonitrile (AN), toluene (TL), methanol, and 0.1 M hydrochloric acid were supplied by Fisher Scientific, UK. Ethylene glycol dimethacrylate (EGDMA), azobis-(isobutyronitrile) (AIBN), and fluorescein isothiocyanate isomer I (FITC) were purchased from Sigma-Aldrich, UK. All the reagents were of analytical grade. A Millipore Milli-Q Plus 185 water purification system was used to supply pure water. All the gases were supplied by BOC, UK with a purity higher than 99.999%.

2.2. Particle Synthesis. The steps in the synthesis of molecularly imprinted poly(AAm-*co*-EGDMA) particles are shown in Figure 1a. The dispersed phase was composed of 60 mmol of EGDMA (cross-linker), 3.6 mmol of AIBN (initiator), 3 mmol of OA (template), and 12−48 mmol of AAm (functional monomer) dissolved in 30 mL of AN (porogen) (Table 1). The continuous phase was a light mineral oil (160 mL). The use of porogen is crucial for the creation of porous polymer networks.[25] AN, toluene, dichloromethane, chloroform or their mixtures have been widely used as porogens in

Table 1. Dispersed Phase Compositions, and the Specific Surface Areas and Pore Volumes of the Synthesized Poly(AAm-co-EGDMA) Particles.[a]

sample	AAm (mmol)	OA (mmol)	EGDMA (mmol)	AIBN (mmol)	S_{BET} (m^2/g)	V_p (cm^3/g)
S1-MIPs	12	3	60	3.6	187	0.64
S2-MIPs	24	3	60	3.6	168	0.43
S3-MIPs	48	3	60	3.6	88	0.27
S3-NIPs	48		60	3.6	127	0.39
S-EGDMA			60	3.6		

[a] S_{BET} is the specific surface area and V_p is the pore volume. Continuous phase: 160 mL of light mineral oil; Porogenic solvent: 30 mL of AN; Polymerization time: 3 h; Polymerization temperature: 60 °C; Agitation speed: 800 rpm.

DOI: 10.1021/acs.est.7b03259
Environ. Sci. Technol. 2017, 51, 11476−11483

O/W suspension polymerization. Since the porogen should not be miscible with the continuous phase, AN was selected as a porogen in this work.[25,29]

The particle production involved four main steps, as follows:

(1) Monomer−template Self-Assembly. At ambient temperature, CO_2 has a low solubility in AN, and cannot be used as a template. Therefore, OA, which is a structural analogue of two CO_2 molecules, was selected as a dummy template. AAm and OA were dissolved in AN; the mixture was stirred for 15 min and then left overnight to allow the self-assembly of OA and AAm into a prepolymerization complex (Figure 1b, step I). The distance between the adjacent NH moieties in the OA-AAm complex is 0.45−0.7 nm,[24] which is an ideal spacing for hydrogen bonding with CO_2 molecules, which have a kinematic diameter of 0.33 nm.[30]

(2) O/O Suspension Polymerization. The mineral oil was poured into a 500 mL jacketed reactor equipped with a four-neck lid, and heated to 60 °C using a water-recirculating heater/chiller system, while agitated by a four-bladed impeller with a diameter of 50 mm. The prepolymerization solution was prepared by dissolving EGDMA and AIBN in the preblended OA-AAM mixture, and then added to the reactor to initiate the reaction (Figure 1b, step II). The emulsion was purged with nitrogen for 10 min, followed by nitrogen blanketing throughout the entire polymerization to ensure the absence of oxygen. The nonimprinted polymer (NIP) particles have been synthesized using the same procedure, except that no template was used.

(3) Mineral Oil Removal. After the polymerization, the mineral oil was separated from the suspension by centrifugation for 20 min at 3500 rpm using a Heraeus Labofuge 400 centrifuge (ThermoFisher Scientific Inc., Germany). The particles were then washed with toluene to remove the remaining mineral oil, rinsed with methanol, filtered in a Buchner funnel using a Whatman grade 1 filter paper and dried overnight in a vacuum oven at 80 °C.

(4) Template Removal. The template was removed from the polymer matrix by washing the particles with a 10/90 (v/v) mixture of 0.1 M hydrochloric acid and methanol, until no traces of OA were detected in the wash water by a Lambda 35 UV/Vis spectrometer (PerkinElmer, US). The particles were then washed with methanol, filtered in a Buchner funnel and dried overnight under vacuum at 80 °C. The extraction of OA from the particles creates amide-decorated cavities with CO_2 recognition properties within the polymer network (Figure 1b, step III). These cavities differ from the pores formed due to the phase separation between the porogen and the polymer during polymerization.[31]

2.3. PARTICLE CHARACTERIZATION

Confocal Laser Scanning Microscopy (CLSM). The texture of the particles was visualized using a Nikon Eclipse TE300 confocal inverted microscope connected to a computer running Zeiss LaserSharp 2000 software. The fluorescent particles were synthesized by adding FITC into the prepolymerization mixture. The stained particles were placed on a microscope slide, and the FITC was excited with an argon laser at a wavelength of 492 nm and a helium−neon laser with a wavelength of 518 nm. The emitted fluorescence was detected by a photomultiplier tube at 515 ± 30 nm (the green region).

Adsorption Isotherms of CO_2 and N_2. The adsorption isotherms of CO_2 and N_2 in the pressure range of 0−1 bar and at temperatures of 273 and 298 K were obtained using a Micromeritics ASAP 2020 static volumetric apparatus equipped with a Micromeritics ISO Controller. Prior to each test, the particles were degassed under vacuum at 80 °C overnight.

Detailed descriptions of other material characterizations methods used in this work are provided in Supporting Information (SI) S1.

3. RESULTS AND DISCUSSION

3.1. Particle Synthesis and Size Control. The size of the particles was controlled by adjusting the stirring speed during the polymerization. The SEM images of the synthesized particles at different stirring speeds are shown in Figure 2a−d. An increase in the stirring speed from 300 to 1200 rpm caused a reduction in the median particle diameter from 1208 to 375 μm. The higher agitation speeds created a higher shear stress at the interface, resulting in smaller particle sizes.[27] The particles produced at agitation speeds of 600−1200 rpm, with a density of 1.3 g cm^{-3} and a diameter up to 800 μm, belong to Group B of the Geldart classification,[32] known as "sandlike" or granular particles. These particles are generally easy to fluidize, with negligible channeling and spouting only in shallow beds, but they tend to form gas bubbles as soon as they are fluidized.

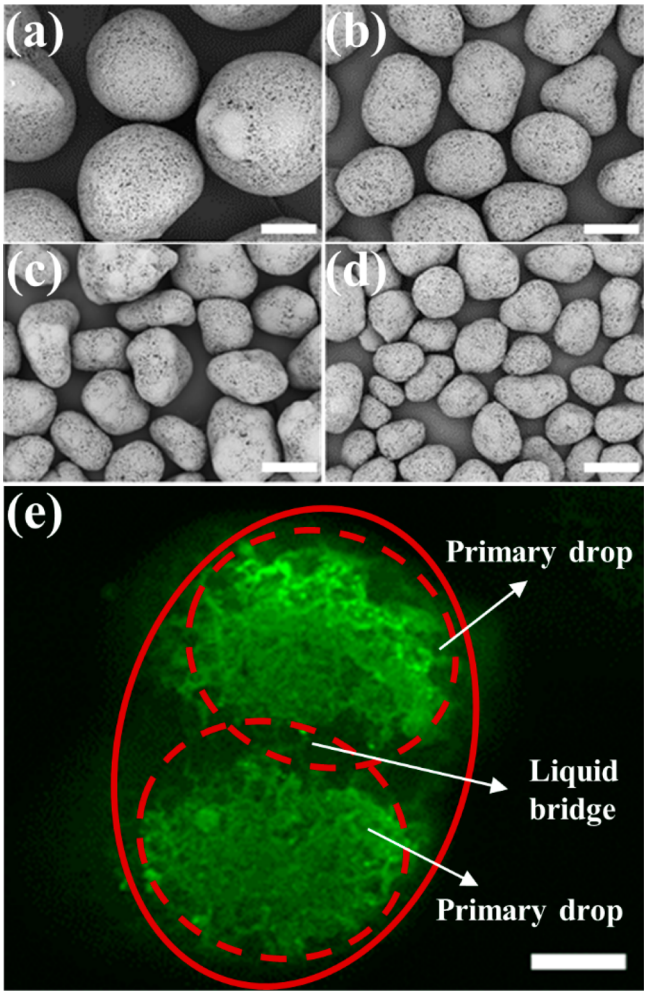

Figure 2. (a-d) The effect of agitation speed on the morphology of S2-MIP particles: (a) 300 rpm; (b) 600 rpm; (c) 800 rpm; (d) 1000 rpm. (e) CLSM images of S2-MIPs formed from the droplets that experienced arrested coalescence. The scale bar for (a)−(d) is 500 μm, and for (e) is 100 μm.

DOI: 10.1021/acs.est.7b03259
Environ. Sci. Technol. 2017, 51, 11476−11483

The particles produced at 300 rpm with a diameter of 1208 μm are more difficult to fluidize and belong to Group D, spoutable particles. The production yield of S1-MIPs, S2-MIPs, and S3-MIPs of 78%, 88%, and 91%, respectively, was significantly greater than that of MIPs synthesized through bulk polymerization, in which case only 30−40% of the particles can be recovered after sieving.[25]

The synthesized particles are nonspherical and have an irregular shape, but with no sharp corners or edges, which make them structurally robust and stable against mechanical attrition. The irregular shape of the particles can be attributed to the partial coalescence of droplets during polymerization and formation of stable, nonspherical aggregates of two or more drops,[33] which is known as arrested coalescence. Due to agitation in the reactor, droplets collide with each other, which can lead to their coalescence. During coalescence, two drops merge via the formation of an infinitesimal liquid bridge between them, which then expands to the size of the drops due to high Laplace pressure at the point of contact.[34] A complete fusion of the coalescing drops into a single spherical drop can be arrested in an intermediate shape if the Laplace pressure is offset by a rheological resistance. In Pickering emulsions, droplets can experience arrested coalescence due to jamming of closely packed particles at the interface. In that case, the Laplace stress within the arrested structure is balanced by the elastic modulus of the jammed particles.[35] In this work, however, coalescence was arrested as a result of internal elasticity of partially polymerized semisolid drops that offsets the interfacial pressure driving two drops to minimize their surface area and interfacial energy. Although no surfactant was added to the mineral oil, the interfacial driving force was rather low due to low interfacial tension (5.12 mN m^{-1}), which additionally stabilized the arrested structures. Previous work showed that viscoelastic droplets containing an elastic network of crystals or semisolid wax particles can be prone to arrested coalescence, creating a range of nonspherical cluster shapes.[36]

The number of connections formed between drops in the Pickering type arrest is limited due to a limited number of interfacial particles. Droplets with an internal viscoelastic resistance are more flexible in their ability to form multiple connections between drops, even after an initial arrest event.[36] Restructuring of arrested drops occurs as a result of liquid meniscus expansion that drives the drops to relocate to denser clusters. Particles formed from multidroplet clusters with various angles between individual drops are visible in Figure 2a−d. Some drops formed triangular packings with ∼60° angles between them, which are energetically more favorable structures than a two-drop assembly shown in Figure 2e. The anisotropy of multidroplet structures significantly adds versatility to the final particle shapes because of the multiplicity of orientations possible for the third and any subsequent drop in the cluster. Anisotropic MIP particles have a lower packing density compared to regular spheres, which in combination with their relatively high true density and large size, make them well suited for use in conventional CO_2 capture systems compared to highly porous adsorbents, such as activated carbon and MOFs.[37]

Figure 2e is a CLSM image of a nonspherical particle formed by polymerization of a droplet doublet. The region with low intensity of excitation light (denoted as liquid bridge) corresponds to trapped mineral oil within the particle, which was removed during washing. It is known that the distance between the individual drops in arrested structures may vary significantly; some drops may be quite closely packed while others may have a surprising amount of space between them.[36]

3.2. Surface Analysis of Synthesized Particles. Nitrogen adsorption−desorption isotherms and pore size distributions of the samples at 77 K are shown in SI Figure s.1. All samples followed the type II isotherm according to the IUPAC classification,[38] which corresponds to multilayer adsorption on nonporous/macroporous solids. The adsorption initially follows a Langmuir isotherm and the plateau region corresponds to monolayer coverage. A monolayer is completed near the point of inflection at the relative pressure of 0.2−0.3, after which adsorption occurs in successive layers. The pore size distribution data revealed that the samples had a variety of pores over the range of 2−80 nm, with a sharp peak at around 3.7 nm. The measured specific surface area, S_{BET}, and pore volume, V_p, of the samples are listed in Table 1. An increase in the AAm content in the dispersed phase from 12 to 48 mmol caused a reduction in S_{BET} and V_p from 187 to 88 m^2/g, and 0.64 to 0.27 cm^3/g, respectively. This behavior can be attributed to a reduction in the degree of cross-linking of the polymer.[12,24]

The IR spectra of the samples are presented in Figure 3a. An increase in the concentration of AAm led to a remarkable increase in the intensity of peaks for N−H stretching (3440 cm^{-1}), bending (1663 cm^{-1}), and wagging (910−665 cm^{-1}) vibrations, implying an increase in the amine content in the polymer matrix of the adsorbents. This observation was confirmed by X-ray photoelectron spectroscopy (XPS) data shown in Figure 3b, in which an increase in AAm concentration resulted in a larger mass fraction of nitrogen at the polymer surface. In addition, no peak over the range of 1680−1640 cm^{-1} was observed in the IR spectra, which confirms that all C═C bonds in EGDMA and AAm are broken, and no monomer or cross-linker is left in the synthesized particles.

Figure 4 shows TGA profiles of the samples. The temperature of onset of intense thermal degradation, T_d for S1-MIPs, S2-MIPs, and S3-MIPs was 351 °C, 365 °C, and 376 °C, respectively. The higher the AAm content in the prepolymerization mixture, the higher the density of amide groups in the polymer network and the higher the T_d value. To further investigate this trend, a polymer based on the S3-MIPs formulation but without any AAm (poly(EGDMA)) was synthesized, S-EGDMA. In comparison with S3-MIPs, T_d of S-EDGMA of 283 °C was almost 25% lower, probably due to the presence of thermally labile ester bonds in EGDMA units, confirming that a higher proportion of AAm monomer in the network results in higher thermal stability of the polymer.

3.3. Imprinting Factor of Synthesized Particles. The performance of the MIP particles was evaluated by means of the imprinting factor, IF, which is the ratio of the equilibrium CO_2 capture capacity of the imprinted polymer, S3-MIPs, to that of its nonimprinted counterpart, S3-NIPs.[39,40] Figure 5a shows the CO_2 adsorption isotherms of S3-MIPs and S3-NIPs at 273 and 298 K. The imprinted sample, owing to the presence of amide-decorated imprinted cavities, had considerably larger CO_2 capture capacities over the entire range of CO_2 partial pressures and at both measured temperatures. Figure 5b shows the variation of IF at 273 and 298 K over the CO_2 partial pressure range of 0−1 bar. It can be seen that the lower values of CO_2 partial pressure and adsorption temperature resulted in higher IFs. Over the CO_2 partial pressure of 0−0.15 bar, IF decreased from ∼1.55 to 1.45 at 273 K, and from 1.3 to 1.25 at

DOI: 10.1021/acs.est.7b03259
Environ. Sci. Technol. 2017, 51, 11476−11483

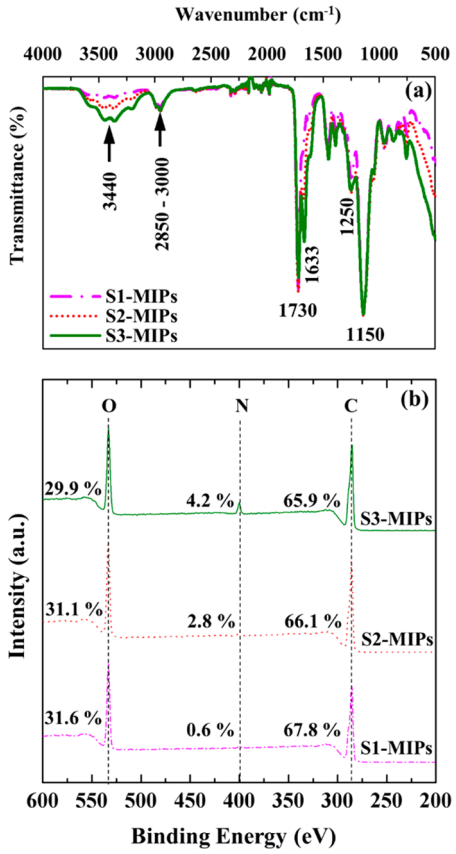

Figure 3. Surface chemical analysis of samples: (a) Fourier transform infrared spectroscopy (FTIR) spectra; the peaks at ~3440 cm^{-1}, 1663 cm^{-1}, and over the range of 910−665 cm^{-1} are attributed to the amine N−H stretching, N−H bending, and N−H wagging vibrations, respectively. The spectra at ~1150 cm^{-1} and its shoulder at ~1250 cm^{-1} are due to C−N stretching vibration in AAm. The peak at ~1730 cm^{-1} can be attributed to C═O bonds in EGDMA and AAm. The peaks over the range of 2850−3000 cm^{-1} are attributed to C−H stretching vibration. (b) XPS spectra including the mass percent of carbon, oxygen, and nitrogen.

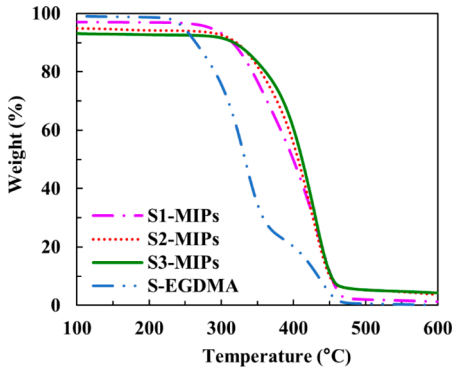

Figure 4. TGA curves of the samples over the temperature range of 150−600 °C, at a temperature rate of 10 °C/min and under nitrogen flow.

298 K. With further increase in CO_2 partial pressure beyond 0.15 bar, a more gradual decrease in IF was seen at 273 K.

3.4. CO_2 Adsorption Capacity and CO_2/N_2 Selectivity. The CO_2 uptake of the synthesized MIPs samples was measured at 273 and 298 K and at CO_2 partial pressures up to 1 bar (Figure 6a and b). The CO_2 adsorption capacity

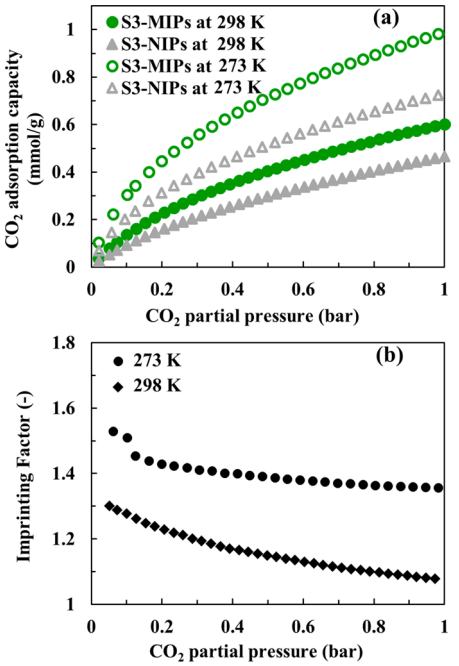

Figure 5. (a) Comparison of CO_2 adsorption isotherms of S3-MIPs and S3-NIPs at 273 and 298 K; (b) The imprinting factors of S3 at 273 and 298 K at CO_2 partial pressures up to 1 bar.

determined from the isotherms at 273 K was 0.9 mmol g^{-1} for S1-MIPs, 1.1 mmol g^{-1} for S2-MIPs, and 1 mmol g^{-1} for S3-MIPs. The CO_2 capture capacity of S2-MIPs and S3-MIPs was similar, but greater than that of S1-MIPs. Since the S_{BET} and V_p values for S1-MIPs were higher than those for S2-MIPs and S3-MIPs, the lower CO_2 capture capacity of S1-MIPs can be attributed to a smaller number of amide interaction sites. At 298 K, the CO_2 capture capacity decreased to 0.51 mmol g^{-1} for S1-MIPs, 0.6 mmol g^{-1} for S2-MIPs, and 0.6 mmol g^{-1} for S3-MIPs. The lower CO_2 capture capacity at higher temperature can be attributed to the weaker dipole−dipole interactions between CO_2 molecules and polar N−H and C═O moieties within the polymer network.[14]

In Figure 6(c) and (d), the CO_2/N_2 selectivity (separation factor), S, of the samples at 273 and 298 K was plotted against CO_2 partial pressure. The S values were calculated from the data points on the CO_2 and N_2 adsorption isotherms shown in Figure 6(a) and (b) using eq 1, based on the Ideal Adsorbed Solution Theory (IAST):[41,42]

$$S = \frac{q_{CO_2}/P_{CO_2}}{q_{N_2}/P_{N_2}} \quad (1)$$

where q and P are the equilibrium adsorption capacity and partial pressure of gas species, respectively. At 273 K and for CO_2 partial pressures of 0−0.2 bar, the highest CO_2/N_2 selectivity of 97−40 was observed for S3-MIPs, followed by 75−38 for S2-MIPs, and 70−37 for S1-MIPs. At CO_2 partial pressures above 0.2 bar, the selectivity was almost identical for all samples. At low partial pressure, the interactions between CO_2 molecules and highly selective CO_2-philic amide groups are crucial for CO_2 uptake, while at higher gas pressures nonselective gas-polymer interactions become increasingly more important.[43] As discussed later, the heat of adsorption of the samples was in the range of 26−32 kJ mol^{-1}, which is within the range of typical enthalpies for the formation of

DOI: 10.1021/acs.est.7b03259
Environ. Sci. Technol. 2017, 51, 11476−11483

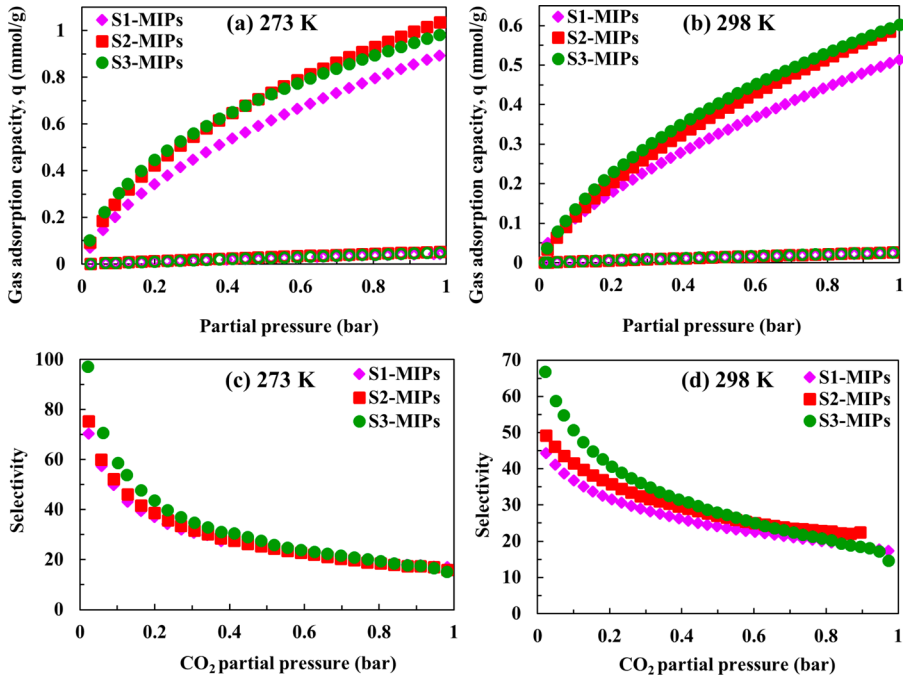

Figure 6. (a) CO_2 and N_2 adsorption isotherms of the samples at 273 K; (b) CO_2 and N_2 adsorption isotherms of the samples at 298 K. The filled and empty symbols represent CO_2 and N_2 adsorption isotherms, respectively. (c) CO_2/N_2 selectivity of the samples at 273 K; (d) CO_2/N_2 selectivity of the samples at 298 K.

hydrogen bonds.[44] When CO_2 interacts with amides, it behaves as both a Lewis acid (LA) and a Lewis base (LB).[45] CO_2 acts as a LA in LA(CO_2)−LB(C═O) interaction and as a LB in hydrogen bonding interaction with the acidic N−H proton.

At low partial pressures, the higher selectivity of S3-MIPs compared to S2-MIPs and S1-MIPs was due to larger number of amide groups available in the polymeric network. On increasing the temperature to 298 K at CO_2 partial pressures of 0−0.2 bar, the selectivity of the samples decreased to 67−40 for S3-MIPs, 53−37 for S2-MIPs, and 44−31 for S1-MIPs. The lower selectivities at higher temperature were due to the weaker interactions of CO_2 with amide groups. Raising temperature increases the kinetic energy of molecules and thus leads to weakening of intermolecular hydrogen bonds.

The purity of the gas stream after regeneration depends on adsorbent selectivity and can be estimated using eq 2:[41]

$$\text{purity} = \frac{q_{CO_2}}{q_{N_2} + q_{CO_2}} \times 100(\%) \quad (2)$$

At a CO_2 partial pressure of 0.15 bar, which is the typical CO_2 concentration of flue gases from coal-fired power stations,[7] the corresponding purities that can be achieved using S3-MIPs, S2-MIPs, and S1-MIPs are 91%, 90%, and 89% at 273 K, and 90%, 89%, and 87% at 298 K. Therefore, S3-MIPs can satisfy the required purity of gas streams for sequestration.[46]

The isosteric heat (enthalpy) of adsorption, Q_{st} (kJ mol^{-1}) was calculated using the Clausius−Clapeyron equation,[47] from the CO_2 isotherm data at 273 and 298 K for different amounts of CO_2 absorbed (Figure 7a). For all samples, Q_{st} was below 32 kJ mol^{-1}, implying physisorptive nature of the adsorption process. In addition, the heat of adsorption was 64% lower than that of aqueous MEA. This implies that all the samples can meet the energy requirement framework defined by the National Energy Technology Laboratory.[11] The highest Q_{st} value was achieved for S3-MIPs, followed by S2-MIPs and S1-MIPs. Higher Q_{st} values are associated with higher affinity toward CO_2. Figure 7b shows the cyclic stability of CO_2 adsorption capacity of S2-MIPs. The adsorption was performed at 298 K and 0.15 bar CO_2 partial pressure, and the desorption

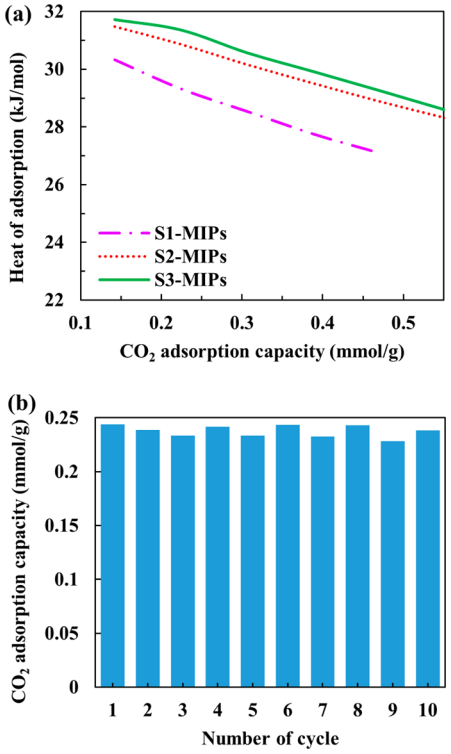

Figure 7. (a) The heat of adsorption of the samples; (b) CO_2 adsorption capacity of S2-MIPs during 10 cycles at 298 K and 0.15 bar CO_2 partial pressure. The desorption was carried out in a stream of pure N_2 at 393 K.

DOI: 10.1021/acs.est.7b03259
Environ. Sci. Technol. 2017, 51, 11476−11483

was carried out in a stream of pure N_2 at 393 K. The CO_2 adsorption capacity was highly stable and there was only a 2.3% reduction in adsorption capacity over 10 consecutive cycles.

In comparison with the reported adsorbents, the MIPs produced in this work benefit from high selectivity. For example, COP-4 (covalent organic polymer) developed by Xiang et al.[20] showed a high CO_2 adsorption capacity of 2 mmol g^{-1} at 298 K and P_{CO2} of 0.15 bar, but their CO_2/N_2 selectivity was below 10. The CO_2 adsorption capacity of the developed MIPs was superior to polystyrene microporous organic polymers (MOPs),[48] and similar to those of CMPs,[49] Azo-COPs-1,[16] PAFs,[50] PPN-6-CH_2CL, and triazine-based polymers (CTFs-TPI-1).[51] However, the CO_2 capture capacity achieved in this work was lower than that of amine-modified porous aromatic frameworks (PAFs) (3.2 mmol g^{-1} for PAF-5 (40 wt % PEI)),[50] and polyamine-tethered porous polymeric networks (PPNs) (3.1 mmol g^{-1} for PPN-6-CH_2DETA).[52] The adsorption capacity of the samples at low partial pressure was relatively low and the future research should show whether it can be further improved, for example, by utilizing amine-based cross-linkers, such as *N*,*N*′-methylenebis(acrylamide). Moreover, since the chemical composition and the mechanism of CO_2 adsorption by the samples are similar to those of impurity-insensitive polymers synthesized by Zhao et al.,[23] it is reasonable to expect that the CO_2 adsorption capacity of the MIPs produced and tested in this work is relatively insensitive to SO_2, NO, O_2, and moisture.

■ ASSOCIATED CONTENT

Supporting Information

The Supporting Information is available free of charge on the ACS Publications website at DOI: 10.1021/acs.est.7b03259.

Description of material characterization methods, nitrogen adsorption−desorption isotherms at 77 K, and pore size distribution curves (PDF)

■ AUTHOR INFORMATION

Corresponding Authors

*(G.T.V.) Phone: +441509222518; e-mail: G.Vladisavljevic@lboro.ac.uk.

*(V.M.) Phone: +44 1234 754649; e-mail: v.manovic@cranfield.ac.uk.

ORCID

Goran T. Vladisavljević: 0000-0002-8894-975X

Notes

The authors declare no competing financial interest.

■ ACKNOWLEDGMENTS

We gratefully acknowledge the financial support for this work by coERCe granted by Innovate UK, project Grant: 102213, and Cambridge Engineering and Analysis Design (CEAD) Ltd. The authors would like to thank Zilin Zhang, Abdulkadir Hussein Sheik, Monika Pietrzak, Rob Bentham, and Kim Robertshaw for their help and support during the entire experimental work.

■ REFERENCES

(1) DECC. CCS Roadmap. Supporting deployment of carbon capture and storage in the UK, 2012.

(2) IEA. CO_2 emissions from fuel combustion highlights; France, 2016.

(3) IEA. Global action to advance carbon capture and storage - a focus on industrial applications; France, 2013.

(4) CCC. Reducing emissions and preparing for climate change: 2015 progress report to parliament summary and recommendations; United Kingdom, 2015.

(5) TUC & CCSA. A UK Vision for Carbon Capture and Storage; United Kingdom, 2013.

(6) Kenarsari, S. D.; Yang, D.; Jiang, G.; Zhang, S.; Wang, J.; Russell, A. G.; Wei, Q.; Fan, M. Review of recent advances in carbon dioxide separation and capture. *RSC Adv.* **2013**, *3* (45), 22739−22773.

(7) D'Alessandro, D. M.; Smit, B.; Long, J. R. Carbon dioxide capture: prospects for new materials. *Angew. Chem., Int. Ed.* **2010**, *49* (35), 6058−6082.

(8) Rochelle, G. T. Amine scrubbing for CO_2 capture. *Science* **2009**, *325* (5948), 1652−1654.

(9) da Silva, E. F.; Booth, A. M. Emissions from postcombustion CO_2 capture plants. *Environ. Sci. Technol.* **2013**, *47* (2), 659−660.

(10) Yu, C. H. A Review of CO_2 capture by absorption and adsorption. *Aerosol Air Qual. Res.* **2012**, *12*, 745−769.

(11) Drage, T. C.; Snape, C. E.; Stevens, L. A.; Wood, J.; Wang, J.; Cooper, A. I.; Dawson, R.; Guo, X.; Satterley, C.; Irons, R. Materials challenges for the development of solid sorbents for post-combustion carbon capture. *J. Mater. Chem.* **2012**, *22* (7), 2815−2823.

(12) Liu, F. Q.; Wang, L.; Huang, Z. G.; Li, C. Q.; Li, W.; Li, R. X.; Li, W. H. Amine-tethered adsorbents based on three-dimensional macroporous silica for CO_2 capture from simulated flue gas and air. *ACS Appl. Mater. Interfaces* **2014**, *6* (6), 4371−4381.

(13) Boot-Handford, M. E.; Abanades, J. C.; Anthony, E. J.; Blunt, M. J.; Brandani, S.; Mac Dowell, N.; Fernández, J. R.; Ferrari, M. C.; Gross, R.; Hallett, J. P.; et al. Carbon capture and storage update. *Energy Environ. Sci.* **2014**, *7*, 130−189.

(14) Nabavi, S. A.; Vladisavljević, G. T.; Wicaksono, A.; Georgiadou, S.; Manović, V. Production of molecularly imprinted polymer particles with amide-decorated cavities for CO_2 capture using membrane emulsification/suspension polymerisation. *Colloids Surf., A* **2017**, *521*, 231−238.

(15) Nabavi, S. A.; Vladisavljević, G. T.; Eguagie, E. M.; Li, B.; Georgiadou, S.; Manović, V. Production of spherical mesoporous molecularly imprinted polymer particles containing tunable amine decorated nanocavities with CO_2 molecule recognition properties. *Chem. Eng. J.* **2016**, *306*, 214−225.

(16) Patel, H. A.; Je, S. H.; Park, J.; Chen, D. P.; Jung, Y.; Yavuz, C. T.; Coskun, A. Unprecedented high-temperature CO_2 selectivity in N_2-phobic nanoporous covalent organic polymers. *Nat. Commun.* **2013**, *4*, 1357−1364.

(17) Mason, J. A.; Sumida, K.; Herm, Z. R.; Krishna, R.; Long, J. R. Evaluating metal-organic frameworks for post-combustion carbon dioxide capture via temperature swing adsorption. *Energy Environ. Sci.* **2011**, *4* (8), 3030−3040.

(18) Remy, T.; Peter, S. A.; Van der Perre, S.; Valvekens, P.; Vos, D. E. De; Baron, G. V.; Denayer, J. F. M. Selective dynamic CO_2 separations on Mg-MOF-74 at low pressures: a detailed comparison with 13X. *J. Phys. Chem. C* **2013**, *117* (18), 9301−9310.

(19) Siriwardane, R. V.; Shen, M. S.; Fisher, E. P.; Poston, J. A. Adsorption of CO_2 on molecular sieves and activated carbon. *Energy Fuels* **2001**, *15* (2), 279−284.

(20) Xiang, Z.; Zhou, X.; Zhou, C.; Zhong, S.; He, X.; Qin, C.; Cao, D. Covalent-organic polymers for carbon dioxide capture. *J. Mater. Chem.* **2012**, *22* (42), 22663−22669.

(21) Choi, W.; Min, K.; Kim, C.; Ko, Y. S.; Jeon, J. W.; Seo, H.; Park, Y. K.; Choi, M. Epoxide-functionalization of polyethyleneimine for synthesis of stable carbon dioxide adsorbent in temperature swing adsorption. *Nat. Commun.* **2016**, *7*, 12640−12648.

(22) Chen, Z.; Deng, S.; Wei, H.; Wang, B.; Huang, J.; Yu, G. Polyethylenimine-impregnated resin for high CO_2 adsorption: An efficient adsorbent for CO_2 capture from simulated flue gas and ambient air. *ACS Appl. Mater. Interfaces* **2013**, *5* (15), 6937−6945.

(23) Zhao, Y.; Shen, Y.; Ma, G.; Hao, R. Adsorption separation of carbon dioxide from flue gas by a molecularly imprinted adsorbent. *Environ. Sci. Technol.* **2014**, *48* (3), 1601−1608.
(24) Zhao, Y.; Shen, Y.; Bai, L.; Hao, R.; Dong, L. Synthesis and CO_2 adsorption properties of molecularly imprinted adsorbents. *Environ. Sci. Technol.* **2012**, *46* (3), 1789−1795.
(25) Chen, L.; Xu, S.; Li, J. Recent advances in molecular imprinting technology: current status, challenges and highlighted applications. *Chem. Soc. Rev.* **2011**, *40* (5), 2922−2942.
(26) Yan, H.; Row, K. H. Characteristic and synthetic approach of molecularly imprinted polymer. *Int. J. Mol. Sci.* **2006**, *7*, 155−178.
(27) Brooks, B. Suspension polymerization processes. *Chem. Eng. Technol.* **2010**, *33* (11), 1737−1744.
(28) Kempe, H.; Kempe, M. Development and evaluation of spherical molecularly imprinted polymer beads. *Anal. Chem.* **2006**, *78* (11), 3659−3666.
(29) Kempe, H.; Kempe, M. Novel method for the synthesis of molecularly imprinted polymer bead libraries. *Macromol. Rapid Commun.* **2004**, *25* (1), 315−320.
(30) Li, J. R.; Kuppler, R. J.; Zhou, H. C. Selective gas adsorption and separation in metal-organic frameworks. *Chem. Soc. Rev.* **2009**, *38* (5), 1477−1504.
(31) Spivak, D. A. Optimization, evaluation, and characterization of molecularly imprinted polymers. *Adv. Drug Delivery Rev.* **2005**, *57* (12), 1779−1794.
(32) Geldart, D. Types of gas fluidization. *Powder Technol.* **1973**, *7* (5), 285−292.
(33) Fredrick, E.; Walstra, P.; Dewettinck, K. Factors governing partial coalescence in oil-in-water emulsions. *Adv. Colloid Interface Sci.* **2010**, *153* (1−2), 30−42.
(34) Paulsen, J. D.; Carmigniani, R.; Kannan, A.; Burton, J. C.; Nagel, S. R. Coalescence of bubbles and drops in an outer fluid. *Nat. Commun.* **2014**, *5*, 3182−3186.
(35) Pawar, A. B.; Caggioni, M.; Ergun, R.; Hartel, R. W.; Spicer, P. T. Arrested coalescence in Pickering emulsions. *Soft Matter* **2011**, *7* (17), 7710−7716.
(36) Dahiya, P.; DeBenedictis, A.; Atherton, T. J.; Caggioni, M.; Prescott, S. W.; Hartel, R. W.; Spicer, P. T. Arrested coalescence of viscoelastic droplets: Triplet shape and restructuring. *Soft Matter* **2017**, *13* (14), 2686−2697.
(37) Liu, J.; Sun, N.; Sun, C.; Liu, H.; Snape, C.; Li, K.; Wei, W.; Sun, Y. Spherical potassium intercalated activated carbon beads for pulverised fuel CO_2 post-combustion capture. *Carbon* **2015**, *94*, 243−255.
(38) Sing, K. S. W.; Everett, D. H.; Haul, R. A. W.; Moscou, L.; Pierotti, R. A.; Rouquérol, J.; Siemieniewska, T. Reporting physisorption data for gas/solid systems with special reference to the determination of surface area and porosity. *Pure Appl. Chem.* **1985**, *57* (4), 603−619.
(39) Dirion, B.; Cobb, Z.; Schillinger, E.; Andersson, L. I.; Sellergren, B. Water-compatible molecularly imprinted polymers obtained via high-throughput synthesis and experimental design. *J. Am. Chem. Soc.* **2003**, *125* (49), 15101−15109.
(40) Gai, Q. Q.; Qu, F.; Liu, Z. J.; Dai, R. J.; Zhang, Y. K. Superparamagnetic lysozyme surface-imprinted polymer prepared by atom transfer radical polymerization and its application for protein separation. *J. Chromatogr. A* **2010**, *1217* (31), 5035−5042.
(41) McDonald, T. M.; Lee, W. R.; Mason, J. A.; Wiers, B. M.; Hong, C. S.; Long, J. R. Capture of carbon dioxide from air and flue gas in the alkylamine-appended metal-organic framework mmen-Mg_2(dobpdc). *J. Am. Chem. Soc.* **2012**, *134* (16), 7056−7065.
(42) Myers, A. L.; Prausnitz, J. M. Thermodynamics of mixed-gas adsorption. *AIChE J.* **1965**, *11* (1), 121−127.
(43) Song, W. C.; Xu, X. K.; Chen, Q.; Zhuang, Z. Z.; Bu, X. H. Nitrogen-rich diaminotriazine-based porous organic polymers for small gas storage and selective uptake. *Polym. Chem.* **2013**, *4* (17), 4690−4696.
(44) Spegazzini, N.; Siesler, H. W.; Ozaki, Y. Activation and thermodynamic parameter study of the heteronuclear C═O···H−N hydrogen bonding of diphenylurethane isomeric structures by FT-IR spectroscopy using the regularized inversion of an eigenvalue problem. *J. Phys. Chem. A* **2012**, *30*, 7797−7808.
(45) Azofra, L. M.; Altarsha, M.; Ruiz-López, M. F.; Ingrosso, F. A theoretical investigation of the CO_2-philicity of amides and carbamides. *Theor. Chem. Acc.* **2013**, *132*, 33−42.
(46) Perera, M.; Gamage, R.; Rathnaweera, T.; Ranathunga, A.; Koay, A.; Choi, X. A Review of CO_2-enhanced oil recovery with a simulated sensitivity analysis. *Energies* **2016**, *9* (7), 481−502.
(47) Kim, H.; Cho, H. J.; Narayanan, S.; Yang, S.; Furukawa, H.; Schiffres, S.; Li, X.; Zhang, Y.-B.; Jiang, J.; Yaghi, O. M.; et al. Characterization of adsorption enthalpy of novel water-stable zeolites and metal-organic frameworks. *Sci. Rep.* **2016**, *6*, 19097−19104.
(48) Kaliva, M.; Armatas, G. S.; Vamvakaki, M. Microporous polystyrene particles for selective carbon dioxide capture. *Langmuir* **2012**, *28* (5), 2690−2695.
(49) Dawson, R.; Adams, D. J.; Cooper, A. I. Chemical tuning of CO_2 sorption in robust nanoporous organic polymers. *Chem. Sci.* **2011**, *2* (6), 1173−1177.
(50) Sung, S.; Suh, M. P. Highly efficient carbon dioxide capture with a porous organic polymer impregnated with polyethylenimine. *J. Mater. Chem. A* **2014**, *2* (33), 13245−13249.
(51) Liebl, M. R.; Senker, J. Microporous functionalized triazine-based polyimides with high CO_2 capture capacity. *Chem. Mater.* **2013**, *25* (6), 970−980.
(52) Lu, W.; Sculley, J. P.; Yuan, D.; Krishna, R.; Wei, Z.; Zhou, H. C. Polyamine-tethered porous polymer networks for carbon dioxide capture from flue gas. *Angew. Chem., Int. Ed.* **2012**, *51* (30), 7480−7484.

DOI: 10.1021/acs.est.7b03259
Environ. Sci. Technol. 2017, 51, 11476−11483